Journal of Hazardous Materials 176 (2010) 109–118

Contents lists available at ScienceDirect

Journal of Hazardous Materials

journal homepage: www.elsevier.com/locate/jhazmat

Removal of nickel on Bofe bentonite calcined clay in porous bed

M.G.A. Vieira [a], A.F. Almeida Neto [a], M.L. Gimenes [b], M.G.C. da Silva [a,*]

[a] UNICAMP/FEQ/DTF, Campinas, SP, Brazil
[b] UEM/CTC/DEQ, Campinas, SP, Brazil

ARTICLE INFO

Article history:
Received 19 June 2009
Received in revised form 29 October 2009
Accepted 30 October 2009
Available online 1 December 2009

Keywords:
Sorption
Bentonite clay
Nickel
Heavy metal removal

ABSTRACT

Bentonite clays have been showing good adsorbing characteristics and are used as an alternative material in the removal of heavy metals. The purpose of this study is to evaluate the removal of nickel on Bofe bentonite calcined clay in porous bed. Firstly, a study was conducted to define the operation outflow, based on the minimum mass transfer zone (MTZ) obtained, useful (q_U) and total adsorbed (q_T) removal amounts and total nickel removal percentage (Rem (%)). Assays of nickel adsorption on clay were conducted according to a 2^2 factorial design with three central points to evaluate the effect of the particle diameter and initial adsorbate concentration on variables q_U, q_T and Rem (%). Tests to obtain the adsorbent physical and chemical characteristics were performed on samples of Bofe clay *in natura*, calcined, and calcined submitted to nickel adsorption. This clay was characterized according to the following techniques: Energy Dispersive Spectroscopy (EDS), Thermogravimetry (TG), Differential Scanning Calorimetry (DSC), X-ray Diffraction (XRD), Fourier Transformed Infrared Spectroscopy (FTIR), Physisorption of N_2 (BET), Helium Picnometry and Scanning Electron Microscope (SEM) with metal mapping.

1. Introduction

Water contamination by heavy metals in industrial effluents is a serious environmental problem. This situation has led to the development of research aiming at its reduction or elimination and at the appreciation of residues obtained through physical, chemical, thermal, biological or mixed ways.

Among heavy metals, nickel is one of the most utilized by western society in the manufacturing process of stainless steel, super alloys, metallic alloys, coins, batteries etc. Direct exposition to nickel causes dermatitis. Some nickel compounds, as carbonyl, are carcinogenic and easily absorbed by skin. The exposure to this compound at an atmospheric concentration of 30 ppm for half an hour is lethal [1].

The existing literature reports many studies on removal of heavy metals from water and effluents, including chemical precipitation, physical treatment such as ion exchange, solvents extraction and adsorption. However, considering the high costs for the maintenance and the importation of chemical products or conventional adsorbents, some methods have become unsustainable.

Several studies have demonstrated that the selectivity and efficiency in the removal of pollution agents, such as heavy metals from effluents through an adsorption process, depend highly on physical properties and chemical composition of the adsorbents.

Recently, the use of clay for sorption or elimination of heavy metals in effluents has been object of study in a great deal of research due to its several economic advantages [2–4]. The cost of these adsorbents is relatively low when compared to other alternative adsorbents, including activated coal, natural and synthetic zeolites, ion-exchange resins and other adsorbent materials. Clay and minerals as montmorillonite, vermiculite, illite, caulinite and bentonite are some natural materials that are being studied as heavy metal adsorbents [5,6]. Another advantage of using clay as an adsorbent is related to its intrinsic properties such as: great specific surface area, excellent physical and chemical stability and several other structural and surface properties [7].

Some types of clay (especially montmorillonite and bentonite) are also widely utilized as barriers in order to avoid contamination of underground water and soil in embankments as a result of lixiviation with heavy metals.

Abollino et al. [8] have observed that Na-montmorillonite adsorbs Cd, Cr, Cu, Mn, Ni, Pb or Zn even when organic substances (bonds) are present. In Covelo et al. [9] Cd, Cr, Cu, Ni, Pb and Zn were adsorbed in mineral clays simultaneously from solutions with several concentrations.

Although the results related to removal of metal in clay are significant and promising, a better understanding of them is needed

* Corresponding author at: State University of Campinas (UNICAMP), School of Chemical Engineering (FEQ), Department of Thermofluidynamic (DTF), Cidade Universitária "Zeferino Vaz", P.O. Box: 6066, 13083-970, Campinas, SP, Brazil.
Tel.: +55 19 35213928; fax: +55 19 35213922.
E-mail address: meuris@feq.unicamp.br (M.G.C. da Silva).

0304-3894/$ – see front matter © 2009 Elsevier B.V. All rights reserved.
doi:10.1016/j.jhazmat.2009.10.128

Nomenclature

C	metal concentration in a solution in the column outlet (ppm)
C_0	initial metal concentration in the liquid state (ppm)
m	dry clay mass (g)
m_{ads}	amount of adsorbed metal per unity of adsorbent mass (mg of adsorbed metal)
q_T	amount of adsorbed metal per unity of adsorbent mass (mg of metal/g of adsorbent)
q_U	amount of adsorbed metal per unity of adsorbent mass up to the breakthrough point (mg of metal/g of adsorbent)
t	time for process (min)
t_b	time until breakthrough point (min)
t_{tot}	time for total removal (min)
V	volumetric outflow of the metal solution (cm^3/min)

regarding adsorbent properties for the optimization of the process conditions.

This study has the purpose of evaluating the removal of nickel on Bofe bentonite calcined clay in porous bed. Initially, a study was conducted to define the operation outflow, based on the minimum mass transfer zone (MTZ) obtained, considering the useful (q_U) and total adsorption (q_T) removal amounts and the total nickel removal percentage (Rem (%)). Assays of nickel adsorption on clay were conducted according to a 2^2 factorial design with three central points to evaluate the effect of the particle diameter and the initial adsorbate concentration on variables q_U, q_T and Rem (%). The adsorbent was characterized in its *in natura* and calcined conditions (before and after the nickel adsorption process).

2. Materials and methods

2.1. Adsorbent clay

In this paper, a Bofe-type bentonite clay from Boa Vista, Paraíba, located in the northeastern region of Brazil, was used. The clay was prepared by size classification, calcined at 500 °C for 24 h in order to increase its mechanical resistance and to eliminate some impurities.

2.2. Metal adsorbate

The adsorption tests were performed using a Ni(II) aqueous solution, generated from $Ni(NO_3)_2{\cdot}6H_2O$ with different concentrations. The Ni(II) solution pH was maintained at a level below minimal precipitation in order to assure the occurrence of the adsorption process only and not the chemical precipitation of nickel ions in the hydroxide form ($Ni(OH)_2$). The study on pH was carried out with HYDRA and by determining the pH_{ZPC}, which corresponds to the zero-point load of solid elements in suspension, using the potentiometrical titration methodology described by Davranche [10] described by Davranche [10]. The pH of the solutions was measured in pH-meters, with automatic temperature compensation and maintaining it at the proper value using nitric acid and ammonium hydroxide.

The concentration of the existing metal in aqueous state of the prepared solutions that were submitted to nickel adsorption assays was determined in the PerkinElmer ANALYST-100 Atomic Absorption Spectrophotometer. The samples were collected using a continued system (Automated Fraction Collector FC 203-Gilson).

2.3. Adsorption experiments

Adsorption experiments were performed in a bed porous system, consisting of an acrylic column 14-cm long and 1.4 cm of internal diameter.

The assays were performed using a mono-compound nickel solution with different concentrations using Bofe calcined clay at 500 °C as adsorbent. The conditions for these assays were defined based on the experimental design, considering the study conducted in batch and preliminary fixed-bed tests.

2.4. Calculation of MTZ, q_U, q_T and removal percentage

In order to determine the mass transfer zone, the amount of useful and total removal were calculated, which correspond to the capacity of metal removal until the breakthrough point (q_U) and saturation point (q_T), respectively. Eqs. (1) and (2) were obtained through mass balance in the column using its saturation data based on its breakthrough curves, where the area below the curve $(1 - C/C_0)$ until the breakthrough point is proportional to q_U, and until the bed exhaustion is proportional to q_T:

$$q_U = \frac{C_0 V}{1000m} \int_0^{tb} \left(1 - \frac{C\big|_{z=L}}{C_0}\right) dt \quad (1)$$

$$q_T = \frac{C_0 V}{1000m} \int_0^{t_{tot}} \left(1 - \frac{C\big|_{z=L}}{C_0}\right) dt \quad (2)$$

MTZ can then be calculated based on the q_U/q_T ratio according to Eq. (3).

$$MTZ = H_L \left(1 - \frac{q_U}{q_T}\right) \quad (3)$$

MTZ has a maximum value which corresponds to the bed height (H_L) and, as the efficacy of mass transference increases, this value decreases until reaching the ideal condition where MTZ is zero and the breakthrough curve is a step function.

The percentage of total removal during adsorption was obtained considering the metal fraction in solution was retained in the adsorbent solid, from total effluent used in the adsorption process until bed saturation.

The amount of adsorbed metal is calculated by considering the curve area $(1 - C/C_0)$ *versus* t [11]. The integral of metal adsorption curves was determined through the *Origin* version 6.0 software.

2.5. Study of outflow and 2^2 factorial design

A preliminary study was conducted with different outflows of 4, 5, 6 and 8 mL/min in order to analyze nickel removal in Bofe calcined clay. The most adequate outflow for this metal removal on clay was determined with basis on results from the analysis on the minimum mass transfer zone, the amount of useful adsorbed metal (q_U), total amount of adsorbed metal (q_T) and the percentage of total metal removal in clay (q_T). Following the outflow definition, the 2^2 factorial design was performed.

A factorial design was proposed with two factors aiming to analyze the influence of clay average particle diameter (d_p) and initial metal concentration (Ni) in aqueous solution (C_0) on nickel adsorption process on Bofe calcined clay. The variables obtained from this study were: useful amount of metal adsorbed on clay (q_U), amount of total adsorbed metal on clay (q_T) and the total metal removal percentage (Rem (%)).

The design included four assays at the coordinates points $x_i = \pm 1$ for both factors (corresponding to the factorial part), besides three repeated tests at the central point ($x_i = 0$), corresponding to average

Table 1
Real and codified values for 2^2 factorial design variables.

Variables	Levels		
	−1	0	+1
d_p (mm)	0.46	0.65	0.855
C_0 (ppm)	50.0	100.0	150.0
C_0 (mmol/L)	0.85	1.70	2.55

values between the variables' inferior and superior levels, totalizing seven tests. Repetitions at the central point have the purpose of supplying a value of pure error and stabilizing the variance of forecasted results.

The diagrams on normal probability as well as the analysis of variance were originated by the STATISTICA® version 7.0 software and it was used as a basis for the interpretation of results obtained experimentally.

Adsorption assays were conducted randomly to avoid systematic error. The assays matrix, its codification and real level of each variable of the fixed-bed adsorption system for nickel on Bofe clay are presented in Table 1.

The inferior level (−1) of the particle diameter of clay was the minimum value obtained that did not cross the contention barrier in the fixed-bed projected column. The superior level (+1) was defined according to the internal column diameter which would not allow the formation of preferential ways during the process.

The superior level of the metal initial concentration in a solution was selected from equilibrium isotherm curves conducted in finite bath. The inferior level of this variable was established according to the legal level required by the Brazilian law (357/2005 – CONAMA), which establishes a 2-ppm concentration of total nickel as the total allowed for standard effluents outflow. Assuming that after removal in porous bed the metal concentration in the outlet is up to 5% of the initial concentration (breakthrough curve point), an initial concentration value around 50 ppm (0.85 mM) can be considered.

2.6. Clay characterization

The physical–chemical characterization of Bofe clay required its chemical analysis by energy dispersive X-ray spectroscopy (EDX), which allows to identify and quantify the total chemical composition of a solid, to determine the surface area by physisorption of N_2 (BET method), real density by helium picnometry, morphological analysis by scanning electron microscopy, identification of particular clay peaks and maintenance of its properties by X-ray diffraction, besides thermal analysis such as thermogravimetry and Differential Scanning Calorimetry (DSC). The above mentioned analyses were performed for samples of Bofe clay *in natura*, calcined and after nickel adsorption. Table 2 shows the analyses types and their respective equipment.

3. Results and discussion

3.1. Nickel speciation and pH_{ZPC}

Supplementary Figure 1 shows the ions Ni^{2+} speciation curve in aqueous solution with nitrate ions at a 0.85 mM (50 ppm) concentration determined by HYDRA. Within the pH range of 6.5–8, the Ni^{2+} ions fraction in aqueous solution decreases and the nickel hydroxide formation, which precipitates, is started. In order to assure the adsorption process only, the pH should be inferior to the minimum precipitation, which, for this concentration (0.85 mM) and ion energy, corresponds to 6.5.

The obtained pH_{ZPC} values for Bofe clay *in natura* and calcined shown in the potentiometric titration curve (Fig. 1) were 6.1 and

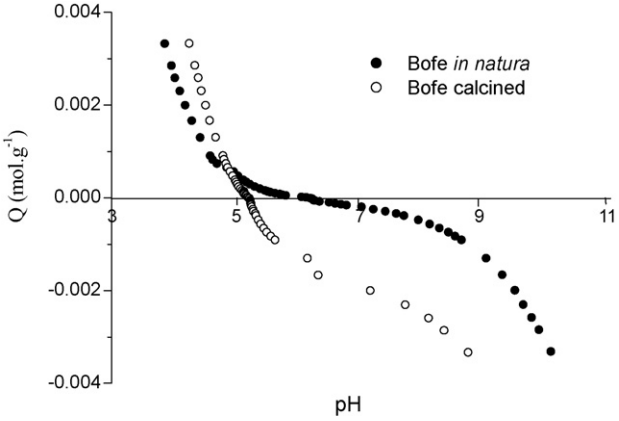

Fig. 1. Potentiometric titration of Bofe clay *in natura* and calcined.

5.3, respectively. The pH for the adsorbate solution was maintained below 5.3 in order to assure zero or negative charge on clay surface as to allow a better adsorption of metal ions with positive charge.

The pH of the dispersions formed by the clays Bofe *in natura* and calcined was measured directly, where one gram of the clay was dispersed in 100 mL of deionized water. The results of this study were 7.78 ± 0.01 and 4.27 ± 0.01 for *in natura* and calcined clay, respectively. The pH of a clay results in part from the nature of exchangeable ions. According to the chemical composition, the exchangeable ions of the *in natura* Bofe clay are cations of alkali metals and alkaline earth metals, which give an alkaline pH to dispersions formed by natural clays. With the calcination, there is no loss of cations, but it occurs the dehydroxylation, which gives an acid pH to the dispersion formed with this state of the Bofe clay.

3.2. Study of outflow for fixed-bed adsorption

In the study carried out based on mass transfer zone, the concentration of nickel adsorbate solution was maintained constant (50 ppm), while the feeding outflow had a 4–6 and 8 mL/min variation.

Fig. 2 shows breakthrough curves in the different outflows studied. It can be noticed that these curves present distinct behaviors indicating the outflow influence on diffusional resistances. The adsorption process presents strong resistance to bed saturation

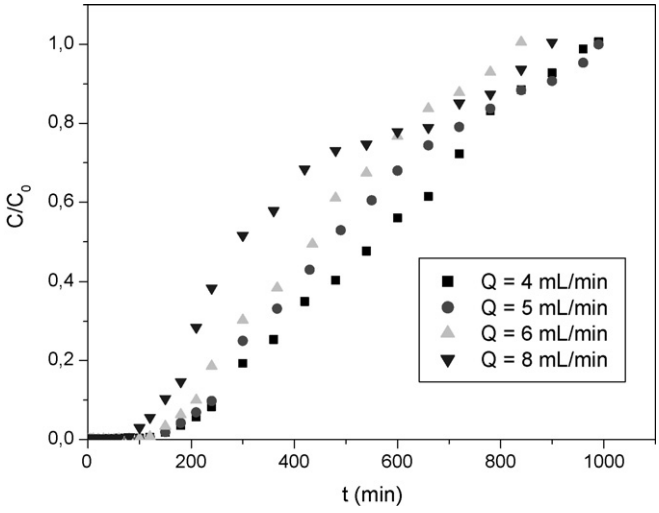

Fig. 2. Breakthrough curves for Ni^{2+}/Bofe calcined clay in different outflows and 50 ppm nickel in solution.

Table 2
Characterization analysis of Bofe clay.

Analysis	Equipment	Parameters/observations
Chemical composition by EDX	EDX, Oxford, 7060 model	Samples received carbon topping
Thermogravimetric analysis (TGA)	TGA-50, Shimadzu	Nitrogen outflow: 50 mL/min; heating rate: 10 °C/min; *T*: 25–1000 °C
Differential scanning calorimetry (DSC)	DSC-50, Shimadzu	Synthetic air outflow: 50 mL/min; heating rate: 10 °C/min; *T*: 25 to 500 °C
X-ray diffraction (XRD)	DRX, Philips, model X'PERT	Cu Kα radiation; voltage: 40 kV; current: 40 mA; step size: 0.020 2θ; time per step: 1.000 s; angle of incidence: 3–50°
Fourier transformed infrared spectroscopy (FTIR)	Spectrum One—FT-IR, PerkinElmer	Adsorption spectra on IR were obtained as KBR pastille form and in the 4000–400 cm^{-1} region
N_2 physisorption (BET)	BET Gemini III 2375 Surface Area Analyser, Micromeritics	N_2 physisorption (BET method) at 77 K
He picnometry	Accupyc 1330, Micromeritics	*T*: 28 °C; equilibrium rate: 0.0010 psig/min
Scanning electron microscopy (SEM)	SEM, model LEO 440i	Vacuum drying (12 h); metallization of samples with gold, utilizing 1 V voltage and 3 nA current for 180 s, in argon atmosphere

Table 3
Values for MTZ, q_U, q_T and removal for nickel adsorption on Bofe clay.

Outflow (mL/min)	MTZ (cm)	q_U (mg/g)	q_T (mg/g)	Rem (%)
4	10.04	1.65	5.84	65.75
5	8.64	2.30	6.00	51.28
6	8.77	2.32	6.20	52.96
8	9.83	2.35	7.90	42.00

for the total outflow range studied, shown by the more extended rupture curves and broader mass transfer zones.

Table 3 shows MTZ values, q_U, q_T and nickel removal percentage on Bofe clay. In the 5 mL/min outflow, the least MTZ value (8.64 cm), as well as satisfactory figures for the amount of adsorbed useful metal (q_U), total (q_T) and total removal percentage were obtained. Then, considering the most adequate outflow, a factorial design for conducting the metal adsorption assays was carried out.

3.3. Removal of nickel from Bofe clay on fixed-bed

The experiments on adsorption of nickel on Bofe clay were conducted randomly according to the 2^2 factorial design shown in Table 1. The effects of the initial metal concentration in aqueous solution and the particle diameter of the used adsorbent on adsorption were evaluated, where the resulting variables were the amount of useful removal quantity (q_U), total removal quantity (q_T) and the total removal percentage. The matrix for the dependent/independent variables and respective results are shown in Table 4.

3.3.1. Effect of the initial metal concentration and particle diameter

The initial concentration of nickel in the effluent varied from 50 ppm (0.85 mM) to 150 ppm (2.55 mM) at a 5 mL/min constant outflow. The effect of the initial metal concentration and particle diameter can be seen in Fig. 3 for particles with 0.855 mm (Fig. 3a) and 0.46 mm (Fig. 3b) diameters and for initial metal concentration of 150 ppm (2.55 mM) (Fig. 3c) and 50 ppm (0.85 mM) (Fig. 3d).

According to the breakthrough curves in Fig. 3, the most concentrated adsorbate nickel solutions (C_0 = 150 ppm) showed a shorter period of time for useful removal and less resistance to saturation when compared to the curves of a less concentrated nickel solution (C_0 = 50 ppm) for the two particle diameters studied. Under higher concentrations the adsorption sites are quickly filled, so useful removal is lower and the solid presents less resistance to saturation. Clay pores were saturated faster when submitted to a greater number of Ni^{2+} ions crossing the fixed-bed.

The influence of particle diameter of the utilized adsorbent, shown in Fig. 3c and d, was evaluated by maintaining a constant concentration and a diameter variation of 0.855 mm to 0.46 mm. The particle diameter does not show a significant effect on the adsorption of nickel in Bofe calcined clay, which could mean that the diffusion in the macropores is not a controlling step in this process. This behavior has also occurred in preliminary assays in finite bath, where the second-order kinetic model was the one which offered the best representation of experimental data, while the intra-particle diffusion model did not show a satisfactory adjustment.

Reproducibility of adsorption assays can be seen in Fig. 4, which shows breakthrough curves resulting from three performed tests at the central point (d_p = 0.65 mm; C_0 = 100 ppm). Based on these tests, a pure error value can be deducted and stabilization of results variance is possible. There is also good consonance of replication curves, which confirms the good reproducibility in the obtained results, with a 2.3% average deviation among them. The curves variation is basically due to axial bed dispersion, not considered in this study.

Table 4
Matrix of variables and results obtained from nickel adsorption assays on calcined Bofe clay.

Assay	Independent variables		Dependent variables						Results	
	d_p (mm) (X_1)		q_U (mg/g) (R_1)		q_T (mg/g) (R_2)		Rem (%) (R_3)		ε_{bed}	MTZ (cm)
			(1)[a]	(2)[a]	(1)[a]	(2)[a]	(1)[a]	(2)[a]		
1 (+1; +1)	0.855	150	2.68	2.18	8.90	8.59	31.43	32.15	0.65	9.78
2 (+1; −1)	0.855	50	2.30	2.18	6.00	5.03	51.28	52.00	0.70	8.64
3 (−1; +1)	0.46	150	3.54	3.20	8.86	8.59	31.63	32.35	0.71	8.40
4 (−1; −1)	0.46	50	3.48	3.20	7.88	5.03	32.96	33.68	0.73	7.82
5 (0; 0)	0.65	100	2.52	2.69	7.46	7.62	37.71	37.55	0.72	9.26
6 (0; 0)	0.65	100	2.25	2.69	7.32	7.62	40.74	37.55	0.66	9.69
7 (0; 0)	0.65	100	2.10	2.69	6.92	7.62	37.13	37.55	0.67	9.76

[a] (1) Experimental value; (2) model predicted value.

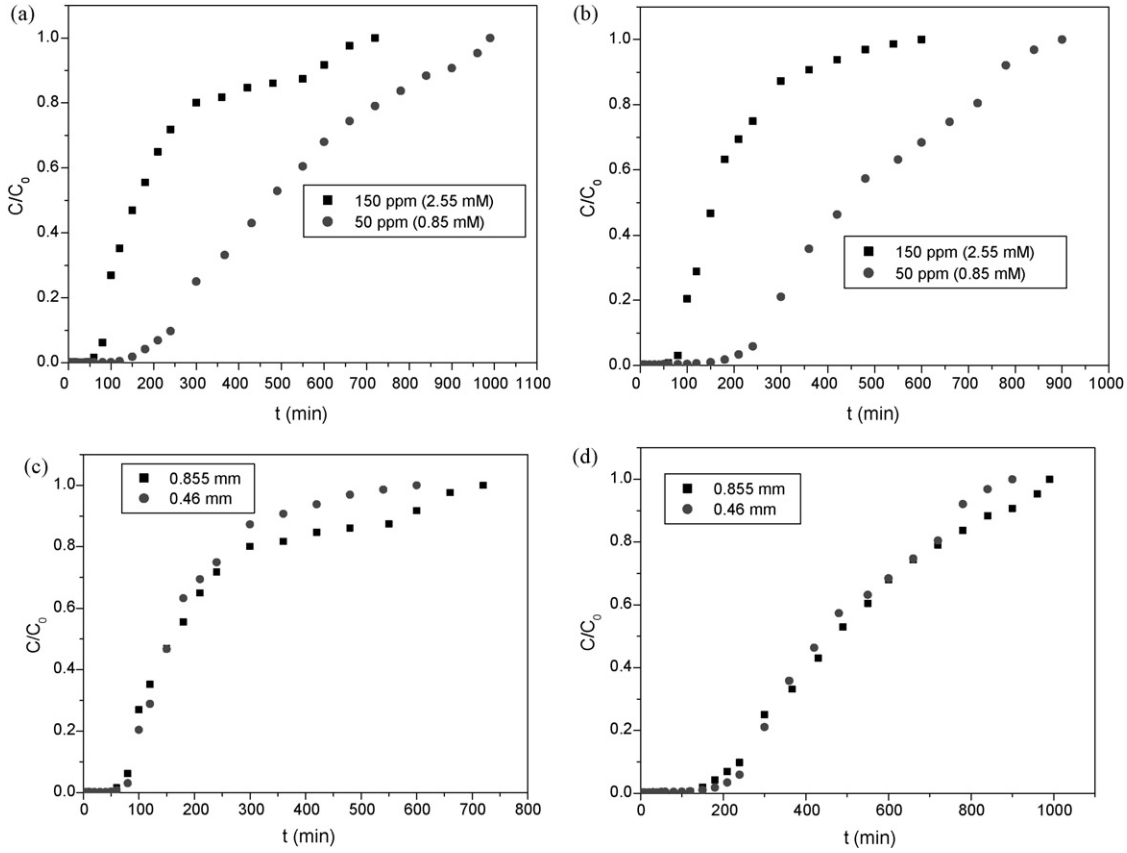

Fig. 3. Effect of the initial metal concentration and of the adsorbent particle diameter on nickel adsorption on calcined Bofe clay: (a) d_p = 0.855 mm; (b) d_p = 0.46 mm; (c) C_0 = 150 ppm; (d) C_0 = 50 ppm.

3.3.2. Statistical analysis of the resulting variables

Considering the statistical analysis results shown in Table 4, the effect of the adsorbing particle diameter and the initial metal concentration in the solution was forecasted for the three response variables (q_U, q_T and Rem (%)).

The statistical significance of individual effects and interaction of the independent variables are confirmed by Pareto's chart, Supplementary Figure 6, where the statistically significant effects are shown on the right of the vertical line that indicates the 95% confidence limit.

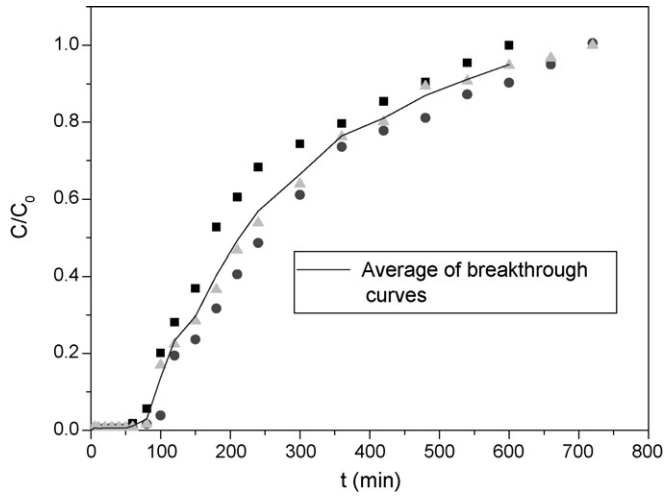

Fig. 4. Reproducibility of breakthrough curves for nickel adsorption on calcined Bofe clay (d_p = 0.65 mm; C_0 = 100 ppm).

Supplementary Figure 6 shows the strong negative influence of particle diameter on the amount of useful removal, while the initial metal concentration presented a positive effect, more expressive in the amount of total metal removal. The removal percentage was influenced by both independent variables, as well as by their interaction, the initial concentration being the most statistically significant. Thus, particles with shorter diameter (d_p = 0.46 mm) showed a greater amount of useful removal, while more concentrated solutions (C_0 = 150 ppm) showed higher values regarding the amount of total removal. As for the total removal percentage, higher values were obtained for less concentrated solutions (C_0 = 50 ppm) and using clay particles with longer diameters (d_p = 0.855 mm) as adsorbent. The interaction of both independent variables had a negative effect on the total removal percentage, since both variables presented opposite effects.

Supplementary Table 5 and Table 5 show results obtained from the analysis of regression coefficients in the codified empiric mathematic models, based on pure error for q_U, q_T and Rem (%) results.

Based on data from Supplementary Table 5 and Table 5 and on Pareto's charts from Figure 6, provided the confidence value is 95%, the empiric codified models, excluding the statistically insignificant ones, were obtained in order to correlate variables with the analyzed results (Eqs. (4) and (6)):

$$q_U = 2.69 - 0.51 \cdot dp \quad (4)$$

$$q_T = 7.62 + 0.97 \cdot C_0 \quad (5)$$

$$\text{Rem}\,(\%) = 37.55 + 4.53 \cdot dp - 5.295 \cdot C_0 - 4.63 \cdot dp \cdot C_0 \quad (6)$$

With the F test (Table 5), it is possible to verify when the obtained regression is significant and if the model lacks fit, since for a good fit, the $F_{calculated}$ for MS_R/MS_r (Mean Square of Regression/Mean Square

Table 5
Analysis of variance for obtained q_U (R_1), q_T (R_2) and Rem (%) (R_3).

Source	Sum of squares (SS)	df	Mean square (MS)	*F*-Value	*p*-Value	$F_{calculated}$ value	F_{table} value
Response 1: q_U (R^2 = 0.5387, R^2 Adj = 0.7715)							
Model: $q_U = 2.69 - 0.51 d_p$							
d_p	1.0404	1	1.0404	22.96689	0.040889	–	–
C_0	0.0484	1	0.0484	1.068433	0.409914	–	–
d_pC_0	0.0256	1	0.0256	0.565121	0.530628	–	–
Regression (*R*)	1.1144	3	0.371467	–	–	MS_R/MS_r	$F_{3,3(\alpha=95\%)}$
Residual (*r*)	0.954771	3	0.318257	–	–	1.17	9.28
Lack of fit (fit)	0.864171	1	0.864171	19.07663	0.048628	MS_{fit}/MS_{pe}	$F_{1,2(\alpha=95\%)}$
Pure error (pe)	0.090600	2	0.045300	–	–	19.07	18.51
Cor. total	2.069171	6	–	–	–	–	–
Response 2: q_T (R^2 = 0.8545, R^2 Adj = 0.70897)							
Model: $q_T = 7.62 + 0.97 C_0$							
d_p	0.8464	1	0.8464	10.77759	0.081591	–	–
C_0	3.7636	1	3.7636	47.9236	0.020235	–	–
d_pC_0	0.9216	1	0.9216	11.73514	0.075669	–	–
Regression (*R*)	5.5316	3	1.8438	–	–	MS_R/MS_r	$F_{3,3(\alpha=95\%)}$
Residual (*r*)	0.942	3	0.314	–	–	5.87	9.28
Lack of fit (fit)	0.784933	1	0.784933	9.994907	0.087168	MS_{fit}/MS_{pe}	$F_{1,2(\alpha=95\%)}$
Pure error (pe)	0.157067	2	0.078533	–	–	9.99	18.51
Cor. total	6.473600	6	–	–	–	–	–
Response 3: Rem (%) (R^2 = 0.9573, R^2 Adj = 0.91465)							
Model: Rem (%) $= 37.55 + 4.53 d_p - 5.295 C_0 - 4.63 d_pC_0$							
d_p	82.0836	1	82.0836	21.84101	0.042863	–	–
C_0	112.1481	1	112.1481	29.84064	0.031916	–	–
d_pC_0	85.7476	1	85.7476	22.81593	0.041143	–	–
Regression (*R*)	279.9793	3	93.32643	–	–	MS_R/MS_r	$F_{3,3(\alpha=95\%)}$
Residual (*r*)	12.4805	3	4.160167	–	–	22.43	9.28
Lack of fit (fit)	4.9640	1	4.9640	1.320835	0.369332	MS_{fit}/MS_{pe}	$F_{1,2(\alpha=95\%)}$
Pure error (pe)	7.5165	2	3.75825	–	–	1.32	18.51
Cor. total	292.4598	6	–	–	–	–	–

of Residual) should be at least twice as great as the F_{table}, while the $F_{calculated}$ for MS_{fit}/MQ_{pe} (Mean Square of Lack of Fit/Mean Square of Pure Error) should be inferior to the respective F_{table} so that the model does not lack fit within the determined confidence interval.

It can also be noticed that the codified model obtained for q_U (Eq. (4)) is not predictable ($MS_R/MS_r = 0.12F_{3,3(\alpha=95\%)}$) and lacks fit ($MS_{fit}/MQ_{pe} > F_{1,2(\alpha=95\%)}$). On the other hand, the regression obtained for q_T (Eq. (5)) is not significant ($MS_R/MS_r = 0.63F_{3,3(\alpha=95\%)}$), although the model does not lack fit ($MS_{fit}/MQ_{pe} < F_{1,2(\alpha=95\%)}$). Finally, the obtained model for the Rem (%) result shown in Eq. (6) is predictable ($MS_R/MS_r = 2.42F_{3,3(\alpha=95\%)}$) and there is no evidence of lack of fit ($MS_{fit}/MQ_{pe} < F_{1,2(\alpha=95\%)}$). The correlation coefficient for Rem (%) was $R^2 = 0.9573$ in relation to the maximum explainable value of 97.43%.

Since the lack of fit of the model expressed by Eq. (4) (q_U) is significant and the regression of the model expressed by Eq. (5) (q_T) is not predictable, only the empiric model expressed by Eq. (6) (Rem (%)) is significant to represent the experimental data. This can be justified because the response Rem (%) is obtained through a global mass balance, i.e., from values at the beginning and at the end of the breakthrough curve. On the other hand, the responses q_U and q_T are determined from a sum of areas, i.e., are subject to variations (experimental deviations) point to point. Therefore, the prediction of these responses by empirical models becomes more difficult when compared to the prediction of the percentage of total removal (Rem (%)).

The effects of independent parameters, d_p and C_0 on the dependent variables q_U, q_T and Rem (%) can be seen on Supplementary Figure 7. Higher values of q_U and q_T were obtained by higher value of C_0 and lower value of d_p, whereas the maximum value of Rem (%) was obtained by lower value of C_0 and higher value of d_p.

The comparison between the experimental and calculated values through the empiric models for q_T and Rem (%) results is shown in Supplementary Figure 8a and b. There is a satisfactory distribution of points around the ideal line for the q_T model and a good distribution of points for the Rem (%) result, confirming, together with the variance analysis, a satisfactory fit between the observed and forecasted values.

Supplementary Figure 8c and d relate forecasted values with their respective residues according to the models, showing that the obtained models (Eqs. (5) and (6)) appropriately represent the variations within these values ranges, since no tendentious distributions of residues can be observed.

3.4. Adsorbent characterization

3.4.1. Chemical composition by EDX

The molecular composition of compounds on Bofe clay *in natura*, calcined and calcined with adsorbed nickel is found in Table 6. The values represent an average of three readings evaluated only qualitatively.

Table 6
Molecular percentage of Bofe *in natura*, calcined and calcined + Ni clay compounds.

Element	% Molecular		
	Bofe clay *in natura*	Calcined Bofe clay	Calcined Bofe clay + Ni
Na	0.54	0.50	–
Mg	1.34	1.19	1.12
Al	7.43	6.84	6.75
Si	46.86	46.17	37.32
K	0.12[a]	–	–
Ca	0.44	0.58	0.29
Ti	0.42	0.53	0.43
Fe	3.58	3.32	3.83
Ni	–	–	0.72
Total	60.85	59.13	49.46

[a] ≤2 sigma.

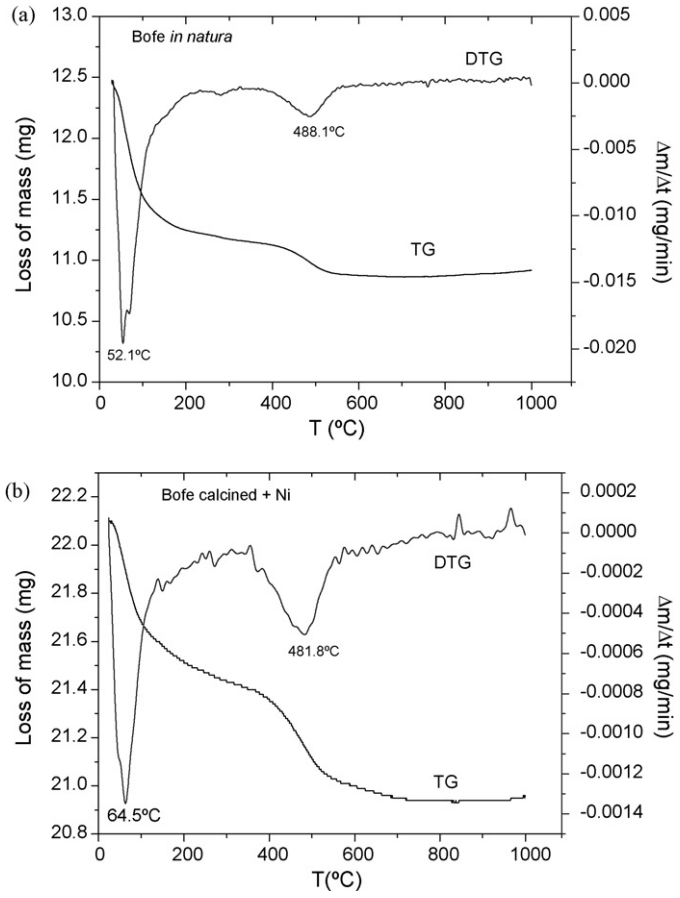

Fig. 5. Thermogravimetric curve up to 1000 °C for Bofe clay: (a) *in natura*; (b) calcined + adsorbed Ni.

All present elements in the average composition, except for nickel, show values similar to those of this clay class, according to Souza Santos' data [12].

When considering the analysis of its chemical composition, Bofe clay can be named polycation bentonite due to the presence of Ca^{2+}, Mg^{2+} and Na^{+} cations in the calcined and *in natura* clays samples. This type of clay is the most found in Brazil.

The quantitative C.E.C. values obtained for Bofe clay "in natura" and calcined are, respectively, 93.333 ± 5.739 and 55.652 ± 4.260. The smectite clays of Paraíba generally have CEC values between 50 and 90 meq/100 g of clay [12]. The comparatively high CEC value of the "in natura" clay indicates that the minerals have a high level of isomorphic substitutions. Moreover the smectite calcined at 500 °C has the ability to exchange cations drastically reduced in relation to the natural clay.

The percentages of elements obtained by EDX demonstrate that practically there was no change in the chemical composition of Bofe clay after its calcination, and the main elements are preserved, such as silicium and aluminium, as well as the exchangeable cations. As a consequence of nickel adsorption, there was a reduction in the number of Ca^{2+} and Mg^{2+} cations and disappearance of Na^{+} cations which may indicate the ionic interchange in the process, mainly for Na^{+}, as it is more easily exchangeable due to its monovalent characteristic.

3.4.2. Thermogravimetric analysis

Fig. 5 shows TG and DTG curves for samples of Bofe clay *in natura* before the adsorption process, calcined and submitted to nickel adsorption. The three samples showed two peaks of mass loss in DTG. The first, around 50–65 °C, refers to the loss of water, volatile compounds, microorganisms and organic material, that is, elements that do not change clay structure. Mass losses occurred for the two samples within this temperature range and are 2.2, 2.7 and 3.0% of initial mass. The second peak, occurring around 480–500 °C, results from hydroxyl loss, which starts to change the clay structure. This loss corresponds to 5.3, 2.6 and 2.2% of initial mass. So, calcination of clay was made at the temperature of 500 °C in order to increase clay stability for its application in fixed-bed adsorption columns.

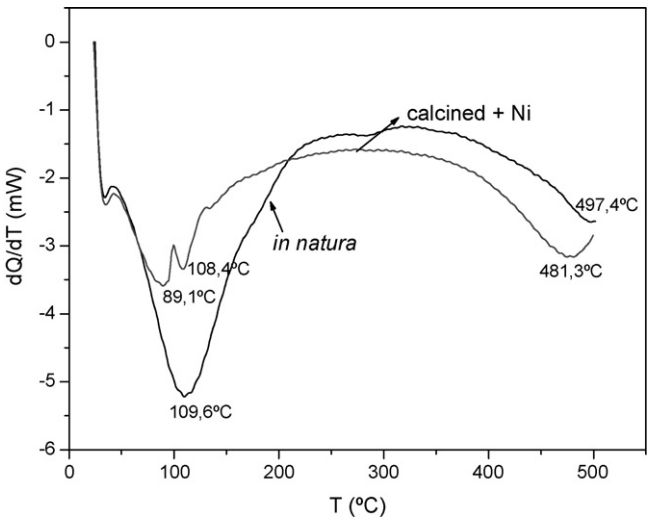

Fig. 6. DSC of Bofe *in natura* and calcined + Ni clays.

3.4.3. Differential scanning calorimetry (DSC)

DSC curves regarding samples of Bofe clay *in natura* before the adsorption process, and calcined clay submitted to nickel adsorption are shown in Fig. 6. The curves show energy bands referring to points of heat absorption due to dehydration and loss of volatiles (first endotherm) and clay dehydroxylation after the calcination process (second endotherm).

If the DSC curves are compared, there is a reduction in the endothermic band at 109.6 °C in the Bofe clay *in natura* sample, which is subdivided into two small endothermic peaks (at 89.1 °C and at 108.4 °C) for the calcined clay with adsorbed nickel sample. A small endotherm can be observed on both curves, occurring for both Bofe clay *in natura* and calcined + Ni samples at temperatures of 497 and 481 °C, respectively.

3.4.4. X-ray diffraction

The XRD analysis for clay samples of Bofe *in natura*, before adsorption, calcination and submission to nickel adsorption are shown in Fig. 7.

In each diffractogram, for the considered band, there are two characteristic peaks for montmorillonite and the others are related to quartz. To easily identify them, the peaks referring to montmorillonite are marked with letter 'M' and the others related to quartz with letter 'Q'.

Considering the angles that correspond to the montmorillonite peaks and applying Bragg's law ($n\lambda = 2d\ \mathrm{sen}\,\theta$), for the λ of 1542 Å value, d is obtained, which represents the basal interlayer distances of Bofe clay, whose results are shown in Table 7.

It can be observed that the Bofe clay samples analysed are not characterized by a highly crystalline structure, as it is found, for example, in zeolites, since the peaks detected in these samples are well defined. The difficulty in identifying peaks is explained by non-diffraction of X-ray, which had a deviation throughout the process,

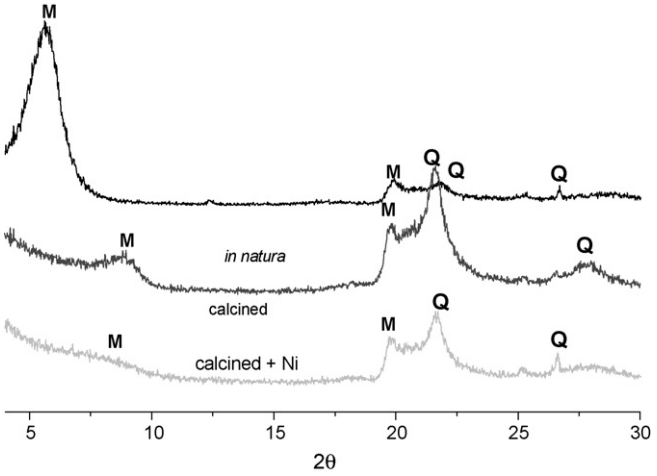

Fig. 7. Diffractogram of Bofe *in natura*, calcined at 500 °C and calcined + Ni adsorbed clays.

what could characterize the formation of an inter-crystalline joint of clays.

Through the diffractograms, there is a significant deviation of the particular montmorillonite peak (Bofe *in natura*) ($2\theta = 5.66^\circ$) for an angle 2θ higher ($8.76^\circ < 2\theta < 8.80^\circ$) obtained for the other samples, which indicates shorter plane interlayer distances (d_{001}), besides a reduction in the peaks intensity in the region $2\theta \approx 20^\circ$ of Bofe calcined clay with adsorbed nickel, in relation to the Bofe calcined clay without this metal.

In Table 7, all samples in the angles of incidence (2θ) between 19.6° and 19.9° regarding the second montmorillonite peak, showed practically the same interlayer basal distances (around 4.5 Å). In the angles of incidence (2θ) between 5.66° and 8.88°, regarding the first montmorillonite peak, the Bofe clay *in natura* sample showed a longer interlayer spacing ($d_{001} = 15.6$ Å) than that of the calcined clay samples (with or without adsorbed Ni), whose values ranged around 10 Å.

3.4.5. Fourier transform infrared spectroscopy

The FTIR spectra for clay samples of Bofe *in natura* calcined, calcined with adsorbed nickel and after four nickel adsorbing/desorbing cycles with various eluents are shown in Fig. 8. The adsorption bands with the corresponding groups and/or bonds for each spectrum are found in Table 8.

FTIR values help to identify possible structural changes occurred in clay after calcination, nickel adsorption and desorption. According to FTIR spectra, it is shown that the band figures that correspond to the OH–stretching remain the same for all samples, in spite of a small deviation in band positions. However, all OH– stretching bands and water molecules existing in *in natura* clay showed reduced intensity after the calcination process. This indicates the occurrence of dehydroxylation and dehydration caused by the thermal treatment of clay at 500 °C [13]. The presence of H_2O is confirmed by the adsorption in approximately 1630 cm^{-1} corresponding to the HOH deformation.

Table 7
Identification of montimorillonite peaks and interlayer distance found by Bragg's method.

Bofe clay	Corresponding angle (2θ-grades)	Basal interlayer distance (Å)
in natura	5.66 19.8	15.61 4.48
Calcined	8.80 19.8	10.05 4.48
Calcined + Ni	8.76 19.6	10.09 4.53

Table 8
Adsorption bands identified on the FTIR spectrum.

Bofe clay	Wave number (cm^{-1}): transmittance	Groups (bond)
in natura	3637 cm^{-1}: 41.5; 3441 cm^{-1}: 31.7 and 1637 cm^{-1}: 53.8	OH– and water
	1098 cm^{-1}: 1.6 and 479 cm^{-1}: 8.8	SiO–
	793 cm^{-1}: 42.6	Quartz
Calcined	3635 cm^{-1}: 56.8; 3428 cm^{-1}: 53.2 and 1637 cm^{-1}: 53.8	OH– and water
	1065 cm^{-1}: 28.7 and 470 cm^{-1}: 33.2	SiO–
	790 cm^{-1}: 62.5	Quartz
Calcined + Ni	3640 cm^{-1}: 63.3436 cm^{-1}: 58.2 and 1636 cm^{-1}: 64.6	OH– and water
	1054 cm^{-1}: 40 and 476 cm^{-1}: 49	SiO–
	794 cm^{-1}: 65.2	Quartz

Bands referring to SiO– bond of *in natura* clay also have their intensity reduced after calcination. The band in 793 cm^{-1} originated by the existence of quartz in Bofe clay did not practically change position after calcination, but showed reduced intensity. Peaks on the 920 cm^{-1} and 800 cm^{-1} bends, like those shown in the spectra, are particular to octahedral layers [14].

The ν_1 and ν_2 bands corresponding to the (Ni)–O bonds occur around 585 and 410 cm^{-1}. The ν_1 adsorption band is caused by metal–oxygen stretching vibration in the tetrahedral regions, while the ν_2 adsorption band is caused by metal–oxygen stretching vibration in the octahedral regions [15]. According to the FTIR spectra obtained for clay samples that contain nickel, no bending band for metal–oxygen bond was observed. Consequently, it may be concluded that nickel removal by calcined Bofe clay was mainly caused by ion exchange between the structures that contain clay tetrahedral and octahedral layers in the clay.

3.4.6. Physisorption of N_2

The obtained values for the surface area by the BET method for clay samples of Bofe *in natura*, calcined and calcined with adsorbed nickel are shown in Table 9, with their respective N_2 adsorption and desorption isotherms and pore diameter based on the increment of intrusion presented in Fig. 9.

This method was chosen as it presents better data adjustment when compared to Langmuir's method, besides having a simi-

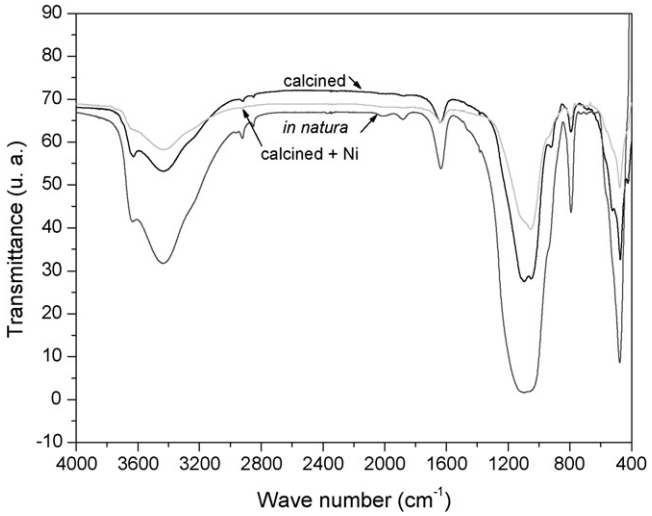

Fig. 8. Spectra for FTIR of Bofe *in natura*; calcined and calcined + Ni clays.

Table 9
Samples surface area calculated by the BET method and real density of Bofe clay, *in natura*, calcined and calcined + Ni.

Bofe clay	BET				Real density (g/cm^3)
	Surface area (m^2/g)	R^2	V_{mi} (cm^3/g)	V_{mes} (cm^3/g)	
*	78.8909	0.9996	19.725	24.560	2.5024 ± 0.0038
Calcined	89.0191	0.9997	21.660	31.945	2.4866 ± 0.0031
Calcined + Ni	92.5897	0.9997	23.356	31.755	2.5316 ± 0.0021

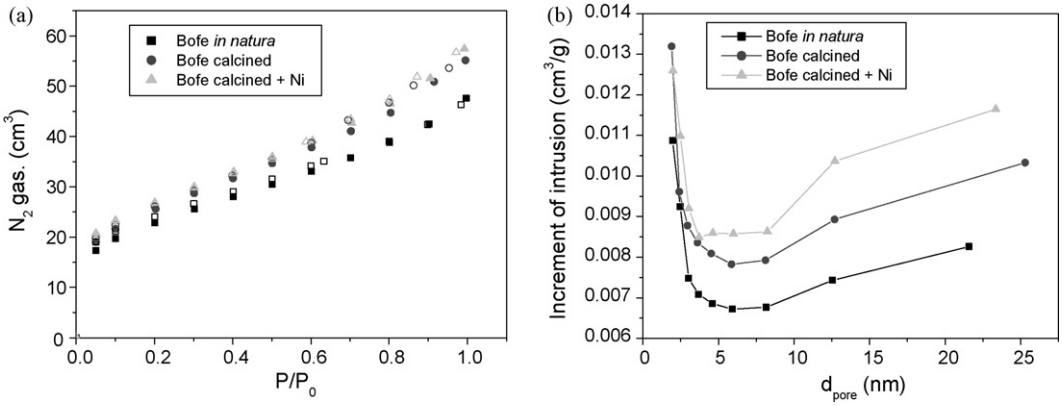

Fig. 9. (a) Adsorption isotherms and N_2 desorption at 77 K. The filled dots represent adsorption and the blank ones, desorption. (b) Increase in intrusion (cm^3/g) *versus* pore diameter (nm) on Bofe clay.

lar behavior in the obtained curves with BET isotherms. This is explainable by the fact that Langmuir's model is more suitable for chemisorption, due to its adsorption restriction in mono-layered processes, while the analysis of nitrogen considers the occurrence of multi-layered adsorption.

Considering BET adsorption isotherms, the micropores (V_{mi}) and the mesopores (V_{mes}) volumes are obtained through the reading of adsorbed volume (V_{ads}) in $P/P_0 = 0.10$ and 0.95 expressed by Eqs. (7) and (8) [16].

$$V_{mi} = V_{ads(P/P_0=0.10)} \quad (7)$$

$$V_{mes} = V_{ads(P/P_0=0.95)} - V_{ads(P/P_0=0.10)} \quad (8)$$

A surface area increase (12.8%) as well as a volume of micropores (9.8%) and mesopores increase (30.1%) in clay after calcinations can be noticed, as a result of loss by dehydration and dehydroxylation. It is possible to consider that calcination may have increased clay microporosity by expanding the micropores upon bond water release, originating pores as mesopores type.

When nickel was adsorbed in clay, there was a slight increase of clay surface area and the development of microporosity (7.8% increase), while the mesopores volume was slightly reduced (0.6%). The replacement of Na^+ Ni^{2+} cations caused an increase of interplanar distance in clay layers, what could justify the surface area increase in clay after the nickel adsorption process.

By analyzing the obtained isotherms, they can be classified according to Brunauer et al. [17] as type II or BET isotherms, characteristic of the multi-layered formation of adsorbed molecules on the solid surface. This type of sigmoidal isotherm (or 'S' shape) is frequently found in non-porous solids or with pores greater than micropores. Bofe clay presented very favorable surface areas for all studied samples.

In Fig. 9a, it is clearly seen that the N_2 desorption isotherm position practically coincides with the adsorption one, i.e., the hysteresis phenomenon which characterizes the irreversibility in the adsorption process can be disregarded for all samples. This indicates that nickel adsorption and desorption in Bofe clay pores is practically reversible [18].

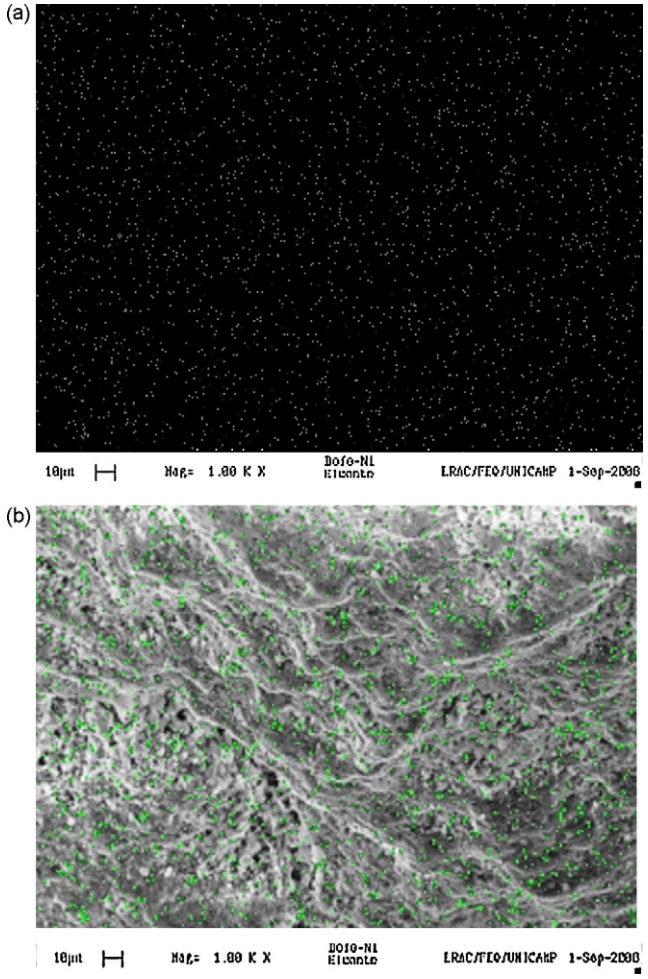

Fig. 10. Metal mapping on Bofe calcined clay ($d_p = 0.855$ mm) with 1000×-amplified: (a) with black background; (b) on image captured by SEM. The dots represent adsorbed nickel on Bofe clay.

According to the classification of pores diameter size [18], pores larger than 50 nm are named macropores, those between 2 and 50 nm are called mesopores and pores with a diameter shorter than 2 nm are named micropores. In Table 9 and Fig. 9b, there are micro and mesopores in all Bofe clay samples with predominant mesoporosity.

3.4.7. Helium picnometry

The real density values regarding Bofe clay *in natura*, calcined before adsorption and calcined submitted to nickel adsorption are found in Table 9. Based on the results, calcination reduces real clay density compared to the *in natura* state. Dehydration and dehydroxilation presented by clay during calcination result in mass loss per volume unit. Nickel adsorption on clay pores causes a slight increase of real density.

3.4.8. Scanning electron microscope with metal mapping

The morphologic analysis of Bofe clay particles by scanning electron microscopy provided the micrograph shown in Fig. 10, whose dots indicate the mapping of the adsorbed nickel on Bofe clay. It can be noticed a homogeneous distribution of the adsorbed nickel throughout the whole surface of clay particle.

4. Conclusions

The most concentrated nickel adsorbate solutions (C_0 = 150 ppm) showed a shorter period of time for the useful removal and less resistance to saturation when compared to the curves of less concentrated nickel solutions (C_0 = 50 ppm) for both particle diameter sizes. The particle diameter did not show a very significant effect in the nickel adsorption on Bofe calcined clay.

A strong negative influence of particle diameter on the useful removal amount was found, while the initial metal concentration showed a more significant positive effect on the amount of total metal removal. The removal percentage was influenced by both independent variables, as well as by their interaction, and the initial concentration was considered the most statistically significant one. Only the empiric model for the Rem (%) result showed to be predictable and did not present lack of fit; in addition, no tendentious distributions of residues were found.

Based on the physical and chemical analysis of Bofe clay, it can be considered poly-cationic and it is not characterized by a highly crystalline structure. The adsorption spectra in the infrared region showed adsorption bands corresponding to the OH– stretching band and water molecules, to the SiO– bonds, as well as to the presence of quartz in clay. Metal–oxygen stretching vibrations in the octahedral and tetrahedral regions were not found, an evidence of ion exchange in the nickel removal process in the interlayer clay structures.

The N_2 physisorption isotherms obtained can be classified as type II or BET, characteristic of multilayered formation composed of adsorbed molecules on the solid surface, typical of non-porous solids or pores greater than the micropores.

Calcination caused the increase of the surface area and the development of clay micro and mesoporosity due to bond water release and dehydroxylation, besides the reduction of real density in relation to the *in natura* state, as a result of the dehydration and dehydroxylation occurred. Nickel adsorption in clay pores caused a slight increase of real density.

Acknowledgements

The authors acknowledge the financial support received from CNPq, CAPES and for State of São Paulo Research Foundation, FAPESP for this study.

Appendix A. Supplementary data

Supplementary data associated with this article can be found, in the online version, at doi:10.1016/j.jhazmat.2009.10.128.

References

[1] R.C.S.S. Seet, A. Johan, C.E.S. Teo, S.L. Gan, K.H.L. Chest, Inhalational nickel carbonyl poisoning in waste processing workers, ProQuest Med. Lib. (2005) 424.
[2] V.R. Ouhadi, R.N. Yong, M. Sedighi, Desorption response and degradation of buffering capability of bentonite, subjected to heavy metal contaminants, Eng. Geol. 85 (1–2) (2006) 102–110.
[3] T. Novakovic, L. Rozic, S. Petrovic, A. Rosic, Synthesis and characterization of acid-activated Serbian smectite clays obtained by statistically designed experiments, Chem. Eng. J. 137 (2) (2008) 436–442.
[4] P. Stathi, K. Litina, D. Gournis, T.S. Giannopoulos, Y. Deligiannakis, Physicochemical study of novel organoclays as heavy metal ion adsorbents for environmental remediation, J. Colloid Interface Sci. 316 (2) (2007) 298–309.
[5] K.G. Bhattacharyya, S.S. Gupta, Adsorption of a few heavy metals on natural and modified kaolinite and montmorillonite: a review, Adv. Colloid Interface 140 (2) (2008) 114–131.
[6] S.M.I. Sajidu, I. Persson, W.R.L. Masamba, E.M.T. Henry, Mechanisms of heavy metal sorption on alkaline clays from Tundulu in Malawi as determined by EXAFS, J. Hazard. Mater. 158 (2–3) (2008) 401–409.
[7] W.J. Chen, L.C. Hsiao, K.K.Y. Chen, Metal desorption from copper(II)/nickel(II)-spiked kaolin as a soil component using plant-derived saponin biosurfactant, Process Biochem. 43 (5) (2008) 488–498.
[8] O. Abollino, M. Aceto, M. Malandrino, C. Sarzanini, E. Mentasti, Adsorption of heavy metals on Na-montmorillonite. Effect of pH and organic substances, Water Res. 37 (7) (2003) 1619–1627.
[9] E.F. Covelo, F.A. Vega, M.L. Andrade, Sorption and desorption of Cd, Cr, Cu, Ni, Pb and Zn by a fibric histosol and its organo-mineral fraction, J. Hazard. Mater. 159 (2–3) (2008) 342–347.
[10] M. Davranche, S. Lacour, F. Bordas, J.C. Bollinger, An easy determination of the surface chemical properties of simple and natural solids, J. Chem. Educ. 80 (1) (2003) 76–78.
[11] B. Volesky, J. Weber, J.M. Park, Continuous-flow metal biosorption in a regenerable *Sargassum* column, Water Res. (2003) 297–306.
[12] P. Souza Santos, Science and Technology of Clays, 2nd ed., In: Edgard Blücher Ltda. (Ed.), 1–3, São Paulo, 1992 (in Portuguese).
[13] K.G. Bhattacharyya, S.S. Gupta, Adsorptive accumulation of Cd(II), Co(II), Cu(II), Pb(II), and Ni(II) from water on montmorillonite: influence of acid activation, J. Colloid Interface Sci. 310 (2) (2007) 411–424.
[14] W.A. Zhang, D.Z. Cheng, H.Y. Xu, X.F. Shen, Y.E. Fang, Influence of four different types of organophilic clay on the morphology and thermal properties of polystyrene/clay nanocomposites prepared using the γ-ray irradiation technique, Eur. Polym. J. 39 (2003) 2323–2328.
[15] R.D. Walorow, Infrared Spectra of ferrites, Phys. Rev. 99 (1955) 1727–1735.
[16] J.G. Gomez, A.M. Garcia, M.A.D. Diez, C.G. Garcia, E.S. Rey, Preparation and characterization of activated carbons from impregnation pitch by $ZnCl_2$, Appl. Surf. Sci. 252 (2006) 5976–5979.
[17] S. Brunauer, P.H. Emmet, E. Teller, Adsorption of gases in multimolecular layers, J. Am. Chem. Soc. 60 (1938) 309–319.
[18] IUPAC, Physical Chemistry Division, Commission on Colloid and Surface Chemistry including Catalysis, Reporting physisorption data for gas/solid systems with special reference to the determination of surface area and porosity, Pure Appl. Chem. 57 (4) (1985) 603–619.